pubs.acs.org/acschemicalbiology

Articles

Guvermectin Biosynthesis Revealing the Key Role of a Phosphoribohydrolase and Structural Insight into the Active Glutamate of a Noncanonical Adenine Phosphoribosyltransferase

Chongxi Liu,‖ Zhiyan Wang,‖ Yin Chen,‖ Yijun Yan, Lei Li, Yong-Jiang Wang, Lu Bai, Shanshan Li, Yanyan Zhang, Xiangjing Wang,* Sheng-Xiong Huang,* and Wensheng Xiang*

Cite This: *ACS Chem. Biol.* 2023, 18, 102−111

Read Online

ACCESS | Metrics & More | Article Recommendations | Supporting Information

ABSTRACT: Guvermectin is a novel plant growth regulator that has been registered as a new agrochemical in China. It is an adenosine analogue with an unusual psicofuranose instead of ribose. Herein, the gene cluster responsible for guvermectin biosynthesis in *Streptomyces caniferus* NEAU6 is identified using gene interruption and heterologous expression experiments. A key intermediate psicofuranine 6′-phosphate (PMP) is chemically synthesized, and the functions of GvmB, C, D, and E are verified by individual stepwise enzyme reactions *in vitro*. The results also show that the biosynthesis of guvermectin is coupled with adenosine production by a single cluster. The higher catalytic efficiency of GvmB on PMP than AMP ensures the effective biosynthesis of guvermectin. Moreover, a phosphoribohydrolase GvmA is employed in the pathway that can hydrolyze AMP but not PMP and shows higher catalytic efficiency for the AMP hydrolysis than that of the AMP dephosphorylation by GvmB, leading to shunting of adenosine biosynthesis toward the production of guvermectin. Finally, the crystal structure of GvmE in complex with the product PMP has been solved. Glu160 at the C-terminal is identified as the acid/base for protonation/deprotonation of N7 of the adenine ring, demonstrating that GvmE is a noncanonical adenine phosphoribosyltransferase.

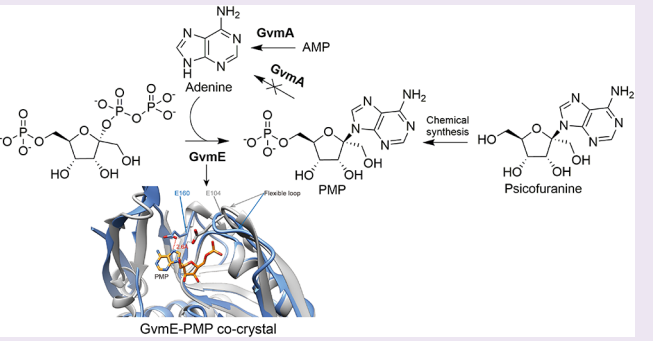

INTRODUCTION

Guvermectin (also known as decoyinine or angustmycin A, **1**) and psicofuranine (also known as angustmycin C, **2**) were originally isolated from *Streptomyces hygroscopius* subsp. *angustmyceticus*[1] and *Streptomyces hygroscopius* subsp. *decoyicus*.[2] They are purine nucleoside antibiotics bearing an unusual psicofuranose connected from C2′ to adenine through a unique C−N glycosidic bond. **1** is distinguished from **2** by elimination of water at psicofuranosyl C5′ and C6′ to form a double bond (Figure 1A). **1** is known to inhibit guanosine monophosphate synthase (GMPS), leading to antibacterial and antitumor activities.[3,4] In 2013, **1** was rediscovered in our laboratory from a plant growth-promoting rhizobacteria *Streptomyces caniferus* NEAU6 and attached great importance to its significant plant growth-promoting activity, which can promote seed germination, tillering, and early maturing in rice. In 2021, we registered it as a new agrochemical in China (registration number PD20212929).

To develop high-yielding strains for the production of guvermectin, we completed the whole genome sequencing of *S. caniferus* NEAU6 in 2016 and started the study on the biosynthesis of **1**. During this period, the gene cluster for **1** biosynthesis was identified in *S. angustmyceticus* NBRC 3934 and *S. decoyicus* NRRL 2666 by Shiraishi et al.[5] Subsequently, the pathway was confirmed by the *in vitro* demonstration that starts with a glycosyl epimerization step from D-fructose 6-phosphate to D-psicose 6-phosphate as catalyzed by AgmD. Subsequent transformations catalyzed by AgmC, AgmE, and AgmB lead to **2**. After the final dehydration catalyzed by AgmF, **2** is converted to **1**.[6] The AgmF-catalyzed reaction resulting in the conversion of **2** to **1** has been elucidated in detail. AgmC, AgmE, and AgmB have also been shown to harbor individual activities of phosphoribosylpyrophosphate synthetase (PRS), adenine phosphoribosyltransferase (APRT), and AMP phosphatase, which together catalyze adenosine production. An excess of adenosine not only leads to a termination of DNA synthesis but also impairs AgmF activity for catalyzing **2** to **1**.[6,7] Therefore, how to coordinate the

Received: September 23, 2022
Accepted: December 27, 2022
Published: January 9, 2023

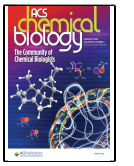

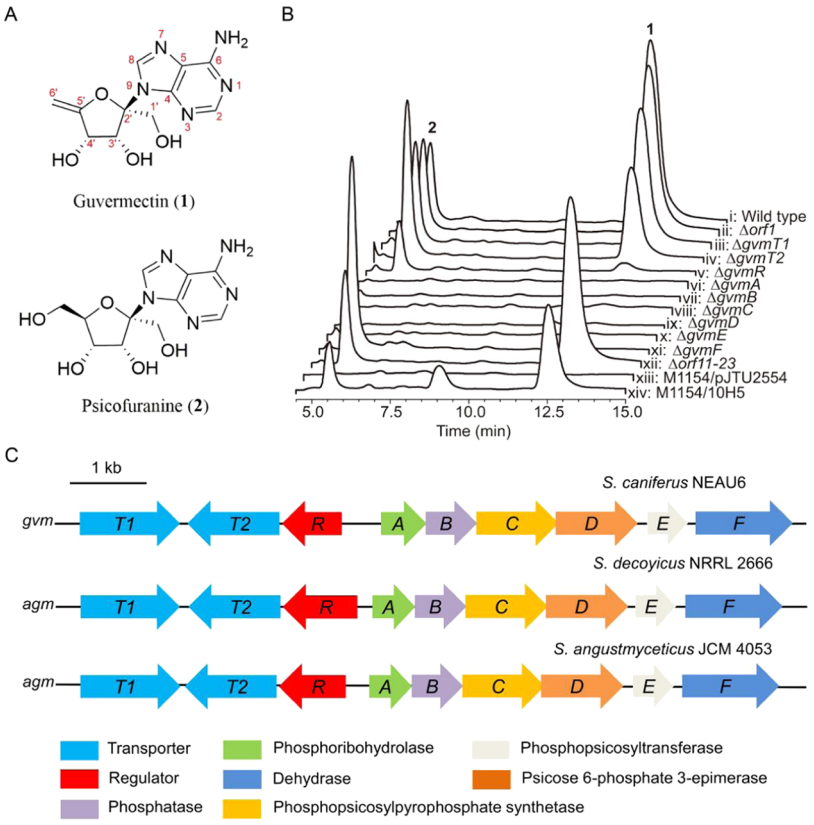

Figure 1. (A) Chemical structures of guvermectin (1) and psicofuranine (2). (B) High-performance liquid chromatography (HPLC) analysis (λ = 260 nm) of the metabolites produced by *Streptomyces coelicolor* M1154/pJTU2554, *S. coelicolor* M1154/10H5, and *S. caniferus* NEAU6 wild-type and mutant strains. (C) Gene organizations of *gvm* and *agm* clusters.

biosynthesis of **1** and adenosine in the pathway remains to be revealed.

In the present study, we identified the gene cluster responsible for the biosynthesis of **1** from *S. caniferus* NEAU6. Then, we synthesized a key intermediate psicofuranine 6′-phosphate (PMP) and reconstructed the biosynthetic pathway through individual stepwise enzyme reactions *in vitro*. Moreover, we performed kinetic analysis to gain insights into the substrate selectivity of GvmA and GvmB, which helps to delineate pathway ordering. Finally, we obtained the cocrystal structure of GvmE in complex with PMP and defined its unique catalytic site.

RESULTS AND DISCUSSION

Determination of the Guvermectin Gene Cluster in *S. caniferus* NEAU6. **1** and **2** were isolated from *S. caniferus* NEAU6 and characterized by HRMS and NMR analysis as well as single-crystal X-ray diffraction (Figures S1−S9 and Table S1, CCDC 2037205 in Cambridge Crystallographic Data Centre). To identify the gene cluster of **1** from *S. caniferus* NEAU6, the genome was sequenced, which generates 9.7 Mb nonredundant data after assembly of clean reads. **1** and **2** are structurally similar to adenosine, implying that they should employ similar enzymatic logic for C−N glycosidic bond formation. Preliminary genomic analysis revealed the presence of two APRT genes. APRT is an essential enzyme responsible for the formation of C−N glycosidic bond in AMP through the transfer of the 5-phosphoribosyl group from 5-phosphoribosyl-1-pyrophosphate (PRPP) to adenine nucleobase in the adenine salvage pathway.[8] Given the high sequence similarity (ca. 80%) of APRT gene present in all *Streptomyces* species, the genuine APRT gene in the adenine salvage pathway in *S. caniferus* NEAU6 could be readily identified. In contrast, the second APRT-like gene (*gvmE*) exhibits only ca. 30% sequence similarity to the genuine APRT gene found in *S. caniferus* NEAU6 (Table S2). Thus, we suspected that *gvmE* might be involved in the biosynthesis of **1**.

To identify the **1** biosynthetic gene cluster, two genomic libraries of *S. caniferus* NEAU6 were constructed using SuperCos1 and pJTU2554 vectors and screened by PCR amplification with primers based on the *gvmE* gene sequence. This effort led to the identification of two cosmids, designated SuperCos1-3E3 and pJTU2554-10H5. The *gvmE* gene was disrupted in *S. caniferus* NEAU6 by insertion of the apramycin resistance gene cassette in cosmid SuperCos1-3E3 using λ-red recombinant technology.[9] The genotype of the mutant was confirmed by PCR (Figure S10). HPLC analysis of the fermentation extract of this mutant indicated that it could not generate **1** and **2** (Figure 1B, trace x), implying that *gvmE* is essential for **1** biosynthesis. To determine the boundaries of the **1** gene cluster, we also inactivated *orf1*, *gvmT1*, *gvmT2*, *gvmR*, *gvmA*, *gvmB*, *gvmC*, *gvmD*, *gvmF*, and *orf11*−*23* genes (Figures S11−S20, respectively). Except for Δ*orf1* and Δ*orf11*-*23* mutants, the production of **1** from all gene inactivation mutants was either abolished or significantly suppressed (Figure 1B, traces ii−ix, xi−xii), thereby suggesting that *gvmT1* and *gvmF* are the terminal genes at the left- and right-hand ends of the **1** gene cluster, respectively. Both *gvmT1* and *gvmT2* encode putative major facilitator superfamily transporters, which are proposed to transport **1** or **2** out of the

https://doi.org/10.1021/acschembio.2c00739
ACS Chem. Biol. 2023, 18, 102−111

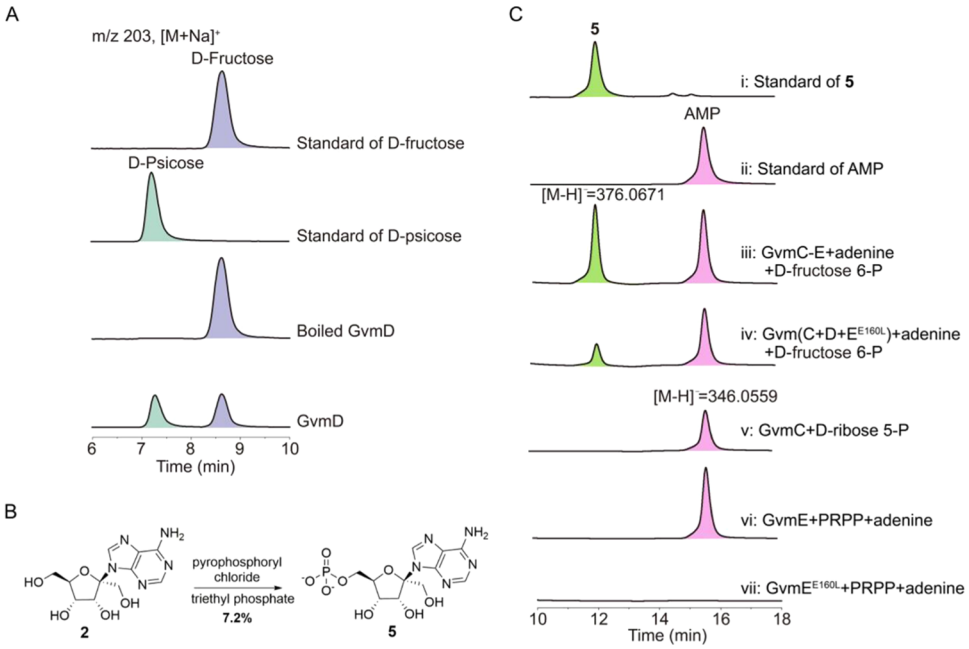

Figure 2. *In vitro* characterization of GvmC, GvmD, and GvmE-catalyzed reactions. (A) LC-MS analysis of *in vitro* GvmD assay. The reaction mixture was dephosphorylated by alkaline phosphatase before LC-MS analysis. (B) Chemical synthesis of PMP (**5**). (C) HPLC traces (λ = 260 nm) showing the reactions of GvmC and GvmE. (i) and (ii) standards of **5** and AMP; (iii) HPLC and HRMS analysis of one-pot *in vitro* reconstitution of **5** biosynthesis using GvmC-E; (iv) HPLC analysis of the reaction of GvmE variant coupled with GvmC and GvmD; (v) HPLC and HRMS analysis of the GvmC-catalyzed reaction with D-ribose 5-phosphate as the substrate; (vi) HPLC analysis of the GvmE-catalyzed reaction with adenine and PRPP as substrates; (vii) HPLC analysis of the GvmE variant-catalyzed reaction with adenine and PRPP as substrates.

producer cell. Inactivation of *gvmR* significantly suppressed the production of **1**, thereby demonstrating that it is a positive transcriptional regulator governing **1** biosynthesis. The Δ*gvmF* mutant abolished the production of **1**, but accumulated **2**, implying that GvmF is responsible for catalyzing the transformation of **2** to **1**. To further characterize this gene cluster, the cosmid pJTU2554-10H5 harboring the genes from *gvmT1* to *gvmF* was transferred into the nonproducing heterologous host *S. coelicolor* M1154 through conjugation. The same conjugal transfer was also performed in parallel using the empty pJTU2554 vector as a negative control. The recombinant *S. coelicolor* M1154/10H5 was fermented using the same medium as had been the case for the wild-type producer. HPLC analysis of the fermentation extract revealed that *S. coelicolor* M1154/10H5 indeed produced **1** and **2**, whereas the control did not (Figure 1B, traces xiii and xiv), demonstrating that the gene cluster spanning *gvmT1* to *gvmF* harbors all of the genes necessary for **1** biosynthesis. This cluster spans ∼8.9 kbp with nine open reading frames (GenBank accession nos. MW126433−MW126441), which are highly homologous to nine genes (*agmT1*, *T2*, *R*, *A*, *B*, *C*, *D*, *E* and *F*, respectively) responsible for the biosynthesis of **1** in *S. decoyicus* NRRL 2666 and *S. angustmyceticus* NBRC 3934 (Figure 1C and Table S3), with sequence identities of 94−99 and 85−92%, respectively.

GvmD Catalyzes the Conversion of D-Fructose 6-Phosphate to D-Psicose 6-Phosphate. BlastP analysis showed that GvmD shares 30% identity to D-psicose 6-phosphate 3-epimerase (ALSE) of *Escherichia coli* K-12, which is known to catalyze the interconversion of D-fructose 6-phosphate and D-psicose 6-phosphate (**3**).[10] Yu et al. found that **1** could still be produced when GvmD was substituted with ALSE in the complete GvmA-F reactions, thus suggesting that GvmD and ALSE share the same functional role.[6] To obtain the direct biochemical evidence that GvmD catalyzes the conversion of D-fructose 6-phosphate to **3**, GvmD was overexpressed and purified from *E. coli* (Figure S21A), and we subsequently evaluated the enzymatic assay of GvmD using D-fructose 6-phosphate as the substrate. However, it is hard to separate **3** from D-fructose 6-phosphate because of its strong polarity. Hence, we dephosphorylated the reaction product using alkaline phosphatase first (Figure S22) and then analyzed it by LC-MS. The expected product D-psicose was observed and confirmed with a standard (Figure 2A).

Promiscuous GvmB, GvmC, and GvmE Enable the Cluster to Produce Both Guvermectin and Adenosine, and the Substrate Selectivity of GvmB Ensures the Effective Biosynthesis of Guvermectin. BlastP analysis showed that GvmC and GvmE are homologous to PRS and APRT, respectively, which are reponsible for AMP biosynthesis in the adenine salvage pathway.[8,11] Earlier studies proposed that GvmC catalyzes the synthesis of 6-phosphoallulosyl-2-pyrophosphate (PPPP, **4**) by transferring the β, γ-pyrophosphate group of ATP to the C2 hydroxyl group of D-psicose, and then GvmE is responsible for the formation of the C−N glycosidic bond in psicofuranine 6′-phosphate (PMP, **5**) through transfer of the 6-phosphoallulosyl group from **4** to adenine in which the signal of **4** was not detected and the structure of **5** was only predicted by LC-MS analysis.[5,6] To further confirm the reactions catalyzed by GvmC and GvmE, the deduced intermediate **5** was chemically synthesized from **2** in this study (Figures 2B and S23−S28); meanwhile, GvmC and GvmE were individually overexpressed and purified from *E. coli* (Figure S21B,C). When GvmC was incubated with the GvmD reaction mixture, a signal at 418.9557 *m*/*z* (negative ion mode) was generated by HRMS analysis (Figure S29A), which matches the predicted mass of the $[M - H]^-$ ion of **4** (418.9551 *m*/*z*). When both GvmC and GvmE were incubated

https://doi.org/10.1021/acschembio.2c00739
ACS Chem. Biol. 2023, 18, 102−111

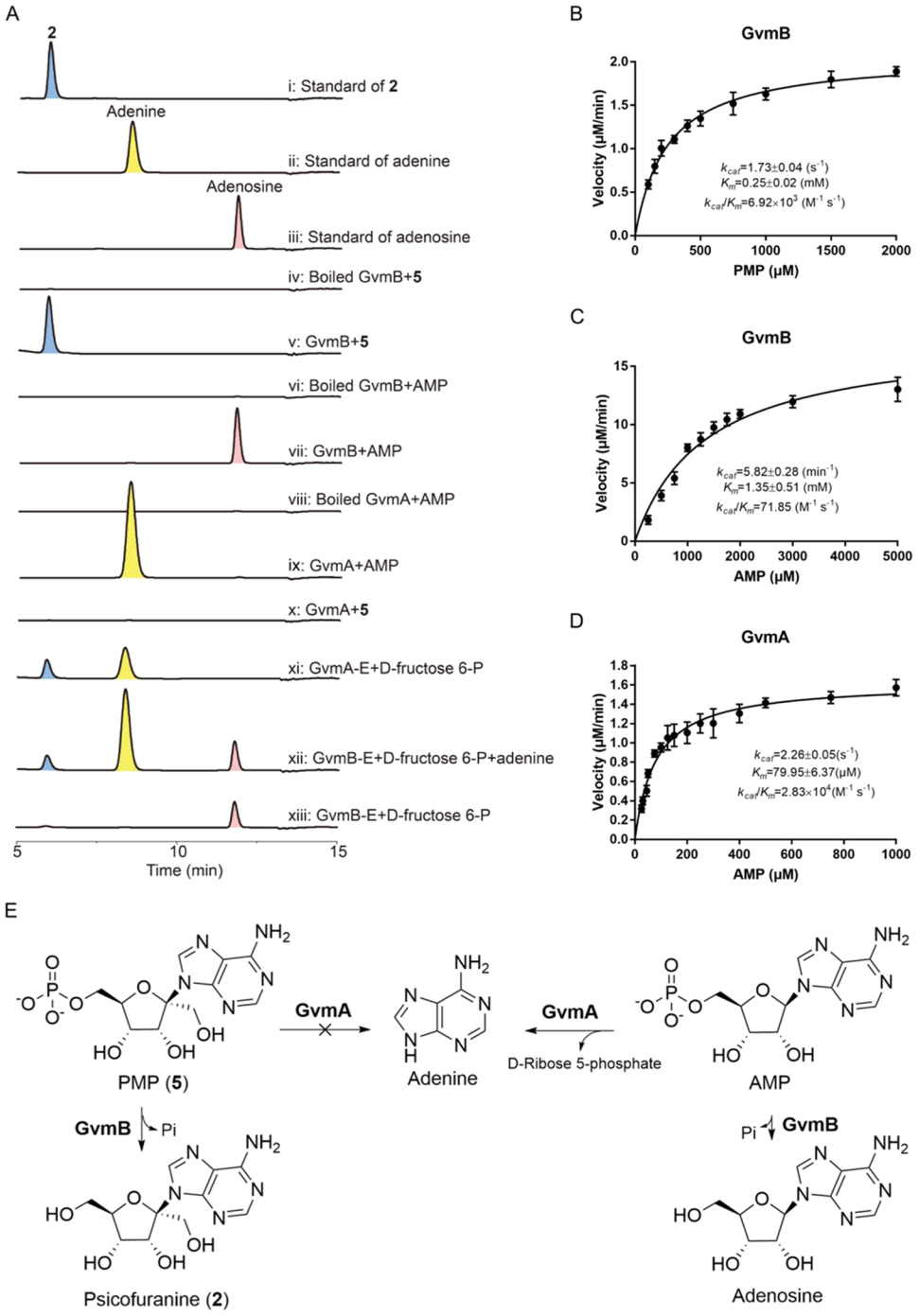

Figure 3. (A) HPLC analysis (λ = 260 nm) of GvmA and GvmB-catalyzed reactions and one-pot reaction *in vitro* for **2** biosynthesis. (i)−(iii) standards of **2**, adenine, and adenosine; (v) HPLC analysis of the GvmB-catalyzed reaction with **5** as the substrate; (vii) HPLC analysis of the GvmB-catalyzed reaction with AMP as the substrate; (ix) HPLC analysis of the GvmA-catalyzed reaction with AMP as the substrate; (x) HPLC analysis of the GvmB-catalyzed reaction with **5** as the substrate; (xi) HPLC analysis of the one-pot reaction *in vitro* for **2** biosynthesis using GvmA-E; (xi) HPLC analysis of the one-pot reaction *in vitro* for **2** biosynthesis using GvmB-E with adenine added; (xii) HPLC analysis of the one-pot reaction *in vitro* for **2** biosynthesis using GvmB-E. (B) Kinetic analysis of GvmB with **5** as the substrate. (C) Kinetic analysis of GvmB with AMP as the substrate. (D) Kinetic analysis of GvmA with AMP as the substrate. (E) Reactions catalyzed by GvmA and GvmB.

with the GvmD reaction mixture, the expected product peak **5** was detected by HPLC analysis and confirmed with HRMS (Figure 2C, trace iii and Figure S29B). GvmC/GvmE was also found to function as PRS/APRT in the adenine salvage pathway.[6] Consistent with this report, incubation of D-ribose 5-phosphate with GvmC along with ATP or incubation of PRPP with GvmE along with adenine led to the production of AMP (Figure 2C, traces v and vi, Figure S29C). The GvmE reaction strongly suggests that the biosynthesis of **1** requires a dephosphorylation enzyme. GvmB, a member of the HAD-like hydrolase superfamily, some of whose members are known to act as phosphatases,[12] is expected to perform the dephosphorylation activity. To test the hypothesis, GvmB was overexpressed and purified from *E. coli* (Figure S21D).

https://doi.org/10.1021/acschembio.2c00739
ACS Chem. Biol. 2023, 18, 102−111

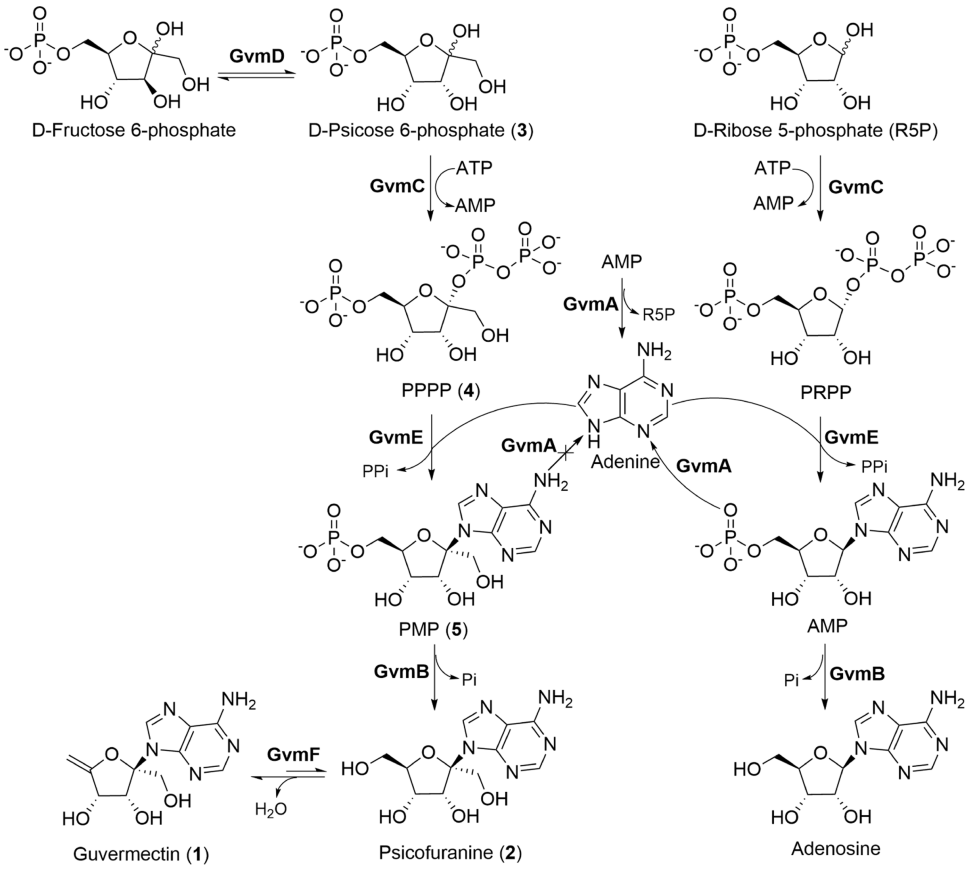

Figure 4. Proposed biosynthetic pathway for **1**.

Incubation of **5** with GvmB led to the production of **2** by HPLC analysis (Figure 3A, trace v). Moreover, GvmB could also catalyze the dephosphorylation of AMP to form adenosine (Figure 3A, trace vii). Functional analysis of GvmB, GvmC, and GvmE suggests that the cluster can also produce adenosine. Enzymatic kinetics analysis indicated that GvmB exhibits higher catalytic efficiency for the conversion of **5** to **2** (k_{cat}/K_m = 6.92 × 10^3 M^{-1} s^{-1}) than that of AMP to adenosine (k_{cat}/K_m = 71.85 M^{-1} s^{-1}) as well as higher substrate affinity toward **5** [K_m (**5**) = 0.25 ± 0.02 mM, K_m (AMP) = 1.35 ± 0.51 mM] (Figure 3B,C). These kinetic properties suggest that GvmB functions in a biosynthetic role to catalyze the dephosphorylation of **5** to **2**, as well as in a protective role to ensure the metabolic stability of **1**.

GvmA Functions to Supply the Substrate Adenine and Alleviate the Substrate Competition for GvmB. The Δ*gvmA* mutant abolished the production of **1** (Figure 1B, trace vi), implying that it plays an important role in the biosynthesis of **1**. GvmA is a homologue of the cytokinin maturating phosphoribohydrolase LONELY GUY-1 (LOG-1) that could hydrolyze AMP into adenine and phosphoribose.[13] To evaluate the functional role of GvmA in the biosynthesis of **1**, it was overexpressed and purified from *E. coli* (Figure S21E). As anticipated, HPLC analysis showed that incubation of GvmA with AMP could generate a peak for adenine, corresponding to an authentic standard (Figure 3A, trace ix). Considering that **5** has a similar structure to AMP, we also tested the enzymatic activity of GvmA against **5** under the same conditions. HPLC analysis revealed that the enzymatic mixture did not yield any detectable product (Figure 3A, trace x). This result demonstrates that GvmA can specifically recognize the substrate AMP but not **5**. AMP can be produced in abundance in the pathway, either from ATP in the GvmC-catalyzed reaction or from ribose 5-phosphate and adenine catalyzed by GvmE. It can also be accepted as a substrate by GvmB. Although **5** is the preferred substrate for GvmB, adenosine was generated in addition to **2** when both **5** and AMP were incubated with GvmB (Figure S30). Single-substrate kinetic analysis revealed that the catalytic efficiency of the AMP hydrolysis by GvmA (k_{cat}/K_m = 2.83 × 10^4 M^{-1} s^{-1}) is 393-fold higher than that of the AMP dephosphorylation by GvmB (Figure 3D), suggesting that the hydrolysis occurs before the dephosphorylation of AMP. Therefore, GvmA plays a key role in alleviating the substrate competition for GvmB and reducing the formation of the byproduct adenosine (Figure 3E). More importantly, adenine, releasing from AMP catalyzed by GvmA, is a substrate for GvmE, hinting that no additional adenine is required in the biosynthetic pathway. To further confirm the role of GvmA in the biosynthesis of **1**, GvmA−E were incubated with D-fructose 6-phosphate and ATP but without adenine, whereupon adenine and the end-product **2** were observed, while adenosine was not detected (Figure 3A, trace xi). In contrast, when GvmA was excluded from the reaction mixture, the production of **2** required the addition of adenine; meanwhile, adenosine was produced in abundance (Figure 3A, traces xii and xiii). GvmA was proposed to be an AMP phosphoribohydrolase for the supply of adenine in the biosynthesis of **1**,[6] consistent with our observation. Here, we propose that the other role of GvmA may be to fine-tune the pathway to prevent the accumulation of excessive adenosine. Finally, the

https://doi.org/10.1021/acschembio.2c00739
ACS Chem. Biol. 2023, 18, 102−111

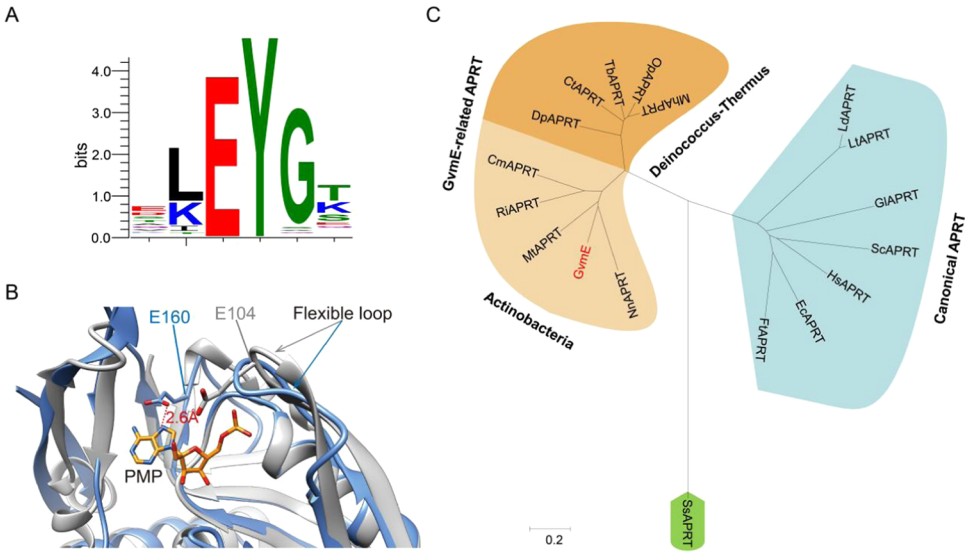

Figure 5. Identification of the catalytic site for GvmE. (A) Sequence logo depicting the conservation of glutamate residue in the flexible loop through multiple sequence alignment of APRT sequences from animals, plants, fungi, protists, bacteria, and archaea. (B) Superimposition of GvmE-PMP (blue) onto the canonical APRT structure (human APRT, PDB: 6FCL, gray). The catalytic Glu160 (blue) in the GvmE protrudes from the C-terminus rather than from the flexible catalytic loop, which is the case for the catalytic important Glu104 (gray) in the human APRT. (C) Phylogenetic analysis of GvmE against other APRTs. The GvmE-related APRT cluster includes NnAPRT (GEM41608) from *Nocardia ninae*, MtAPRT (AYF26665) from *Micromonospora tulbaghiae*, RiAPRT (WP_104265654) from *Rathayibacter iranicus*, CmAPRT (WP_012299566) from *Clavibacter michiganensis*, DpAPRT (WP_027480833) from *Deinococcus pimensis*, OpAPRT (HGY09816) from *Oceanithermus profundus*, CtAPRT (WP_119316072) from *Calidithermus terrae*, MhAPRT (WP_148230415) from *Marinithermus hydrothermalis*, and TbAPRT (WP_244362353) from *Thermus brockianus*. The canonical APRT cluster includes HsAPRT (PDB: 6FCL) from humans, LtAPRT (PDB: 1MZV) from *Leishmania tarentolae*, LdAPRT (PDB: 1QB8) from *Leishmania donovani*, ScAPRT (PDB: 1G2P) from *Saccharomyces cerevisiae*, EcAPRT (PDB: 2DY0) from *E. coli*, GlAPRT (PDB: 1L1Q) from *Giardia lamblia*, and FtAPRT (PDB: 5YW2) from *Francisella tularensis*. SsAPRT (PDB:4TS5) is from *Sulfolobus solfataricus*..

biosynthetic pathway for **1** was determined as shown in Figure 4.

GvmE Represents a Family of APRTs with the Catalytic Glutamate at the C-Terminus. The reaction catalyzed by APRT has been proposed to involve an oxacarbenium transition state in which the adenine leaving group is activated by N7 protonation (Figure S31). In the canonical APRTs, the proton is donated by a conserved glutamate residue (Glu104 in human APRT) located in the flexible catalytic loop (Figure 5A).[14−18] An exception to this rule is the *Sulfolobus solfataricus* APRT in which this catalytic function results from the β-carboxylate of an aspartate residue positioned in the PRPP binding motif.[19] In GvmE, the homologous position in the flexible catalytic loop is occupied by a glycine (Figure S32). To determine the catalytic site in GvmE, the crystal structure of GvmE was determined at 1.95 Å in complex with the reaction product **5** (Figures 5B and S33 and Table 1; PDB ID: 7F06). GvmE is found as a homodimer, and a calcium ion is located at the dimer interface to stabilize the dimerization by interacting with the carboxylates of Glu70 and Glu73 (Figure S33A). The overall structure of GvmE is very similar to those of canonical APRTs with a hood region, a flexible loop, and a core domain. The core domain is a Rossmann fold structure consisting of a four-stranded β-sheet surrounded by four α-helices (Figure S33B). A carboxylate group of Glu160 at the C-terminus that is located in the H-bond distance (2.6 Å) from N7 of the adenine moiety of **5** was suspected of playing a key role in the N7 hydrogen abstraction (Figure 5B). To verify this deduction, we performed selective mutational assay and determined that the GvmE variant E160L dramatically reduced the activity for catalyzing the synthesis of **5** or AMP (Figure 2B, traces iv and vii), thereby demonstrating that this residue indeed plays a role for the catalytic function of this enzyme. Kinetic assay showed E160L decreased the k_{cat}/K_m by three orders of magnitude for PRPP compared with the wild-type enzyme (Figure S34). BlastP analysis showed that GvmE homologues were also distributed in some species of Actinobacteria and Deinococcus-Thermussimilar. A phylogenetic analysis of GvmE against other APRTs showed that the GvmE-related APRTs formed a separate cluster from canonical APRTs (Figure 5C), suggesting that GvmE represents a family of APRTs with the catalytic glutamate at the C-terminus.

CONCLUSIONS

In summary, the gene cluster responsible for the biosynthesis of guvermectin in *S. caniferus* NEAU6 has been identified, and the functions of Gvm (A, B, C, D and E) have been definitively verified *in vitro* by individual stepwise reactions. Moreover, we demonstrate that GvmA and GvmB relieve the potential "excess adenosine" for producing cells, and thus ensuring the effective biosynthesis of guvermectin. Finally, the crystal structure of GvmE in complex with PMP has been identified, and Glu160 is proposed as the adenine proton abstracting residue before its nucleophilic attack to C2-carbon of PPPP or C1-carbon of PRPP, suggesting that GvmE is an unusual APRT. Compared with recent reports, the novelty of this work is mainly reflected in the following three aspects: (1) through *in vitro* assays, the biosynthesis pathway was studied in detail, which confirmed the involvement of all of the intermediates; (2) kinetic studies of GvmA and GvmB revealed how the biosynthesis avoids the accumulation of adenosine in cells; (3) structural characterization demonstrated that GvmE represents

https://doi.org/10.1021/acschembio.2c00739
ACS Chem. Biol. 2023, 18, 102−111

Table 1. Data Collection and Refinement Statistics of GvmE[a]

parameter	GvmE
Data Collection	
space group	*P*1 21 1
cell dimensions	
α, *β*, *γ* (deg)	90.00, 105.11, 90.00
a, *b*, *c* (Å)	42.758, 71.391, 58.704
resolution (Å)	50.0−1.95 (1.98−1.95)
wavelength (Å)	0.979
$R_{p.i.m}$	0.026 (0.201)
R_{merge}	0.042 (0.38)
$I/\delta I$	29.0 (3.1)
completeness (%)	99.6 (96.1)
redundancy	6.6 (5.3)
Refinement	
resolution (Å)	22.91−1.95 (2.04−1.95)
unique reflections	24833 (1205)
R_{work}/R_{free}	0.182/0.216
B-factors	
protein	22.8
ligand	17.4
water	30.2
Ramachandran	
favored (%)	97.7
allowed (%)	2.3
outlier (%)	0.0
root mean square deviations	
bond lengths (Å)	0.009
bond angles (deg)	1.332
no. of atoms	
protein	2662
ligand	50
water	316

[a]Values in parentheses are for the highest-resolution shell.

a new family of APRT, and point mutagenesis confirmed the key role of a Glu residue in catalysis. This study unravels the hidden workings underlying the biosynthesis of guvermectin and lays the foundation for the future improvement in guvermectin production.

MATERIALS AND METHODS

General Materials and Experimental Procedures. All chemicals and enzymes were purchased from commercial sources and used directly. Primer synthesis and DNA sequencing were performed at Beijing Tsingke Bio Tech Co., Ltd. (Beijing China). PCR amplifications were carried out on Bio-Rad T100 thermal cycler (Hercules, CA). Semipreparative HPLC was conducted on a HITACHI Chromaster system, equipped with a DAD detector, a YMC-Triart C_{18} column (250 mm × 10 mm i.d., 5 μm, Japan), at a flow rate of 3.0 mL/min and a column temperature of 25 °C. HPLC analysis was carried out on HITACHI Chromaster system equipped with a DAD detector, a YMC-Triart C 18 column (250 mm × 4.6 mm i.d., 5 μm, Japan), at a flow rate of 1.0 mL/min and a column temperature of 25 °C. Column chromatography (CC) was performed using a HP-20 macroporous absorbent resin (Mitsubishi Chemical Corp, Japan). NMR spectra were recorded in dimethylsulfoxide (DMSO)-d_6 or D_2O using a Bruker AVANCE III-600 or 800 spectrometer (Bruker Corp., Switzerland), and tetramethylsilane was used as the internal standard. LC-MS analysis was conducted on Agilent 1290/6530 system (Agilent Corp.). HRESIMS data were obtained using an Agilent G6230 Q-TOF mass instrument (Agilent Corp.).

Strain Culture Conditions and Plasmids. Bacterial strains and plasmids used in this work are listed in Table S4. *E. coli* strains were grown on LB medium at 30 or 37 °C. *S. caniferus* NEAU6, *S. coelicolor* M1154, *S. coelicolor* M1154/10H5, and *S. caniferus* NEAU6 mutants were cultured on the mannitol soya flour (MS) medium (soybean powder 2%, mannitol 2%, agar 2%, pH 7.2) plates at 30 °C. Tryptic Soy Broth (TSB) was used as the seed medium, and the guvermectin production medium (soybean powder 4%, malt extract 2%, sucrose 1%, $CaCO_3$ 0.3%, pH 7.2−7.4) was used for fermentation. Kanamycin (Kan), chloromycetin, and apramycin (Apr) were added to the media at concentrations of 50, 25, and 50 μg/mL, respectively, if necessary.

Isolation and Identification of Compounds 1 and 2. *S. caniferus* NEAU6 was grown on MS medium for 5 days at 30 °C. Then, it was inoculated into 250-mL baffle Erlenmeyer flasks containing 50 mL of TSB and cultivated for 24 h at 30 °C with shaking at 200 rpm. After that, aliquots (15 mL) of the culture were transferred into 1-L baffled Erlenmeyer flasks filled with 250 mL of the production medium and cultured at 30 °C for 7 days with shaking at 200 rpm. The fermentation broth was centrifuged (4000 rpm, 20 min), and the supernatant subject to a HP-20 resin column, which was washed twice with water and then eluted with 100% MeOH. The eluent was evaporated under reduced pressure at a temperature within 40 °C and then separated by semipreparative HPLC with MeOH−H_2O (15:85, v/v; wavelength, 260 nm). The structures of compounds **1** and **2** were characterized by HRMS and NMR analyses. White needle crystals of compound **1** were obtained from MeOH−H_2O solution. The X-ray diffraction data were collected on a Bruker APEX DUO single-crystal X-ray diffractometer using Cu K*α* radiation.

Compound **1**: ^{1}H NMR (600 MHz, DMSO-d_6) δ 8.15 (s, 1H, H-2), 7.88 (s, 1H, H-8), 3.97 (d, J = 12.3 Hz, 1H, H-1′), 4.20−4.17 (m, 1H, H-1′), 5.06 (d, J = 4.7 Hz, 1H, H-3′), 4.30 (dt, J = 4.6, 2.3 Hz, 1H, H-4′), 4.20−4.17 (m, 1H, H-6′), 4.52 (d, J = 2.1 Hz, 1H, H-6′) ppm. ^{13}C NMR (150 MHz, DMSO-d_6) δ 152.6 (C-2), 148.6 (C-4), 120.3 (C-5), 156.5 (C-6), 139.1 (C-8), 61.4 (C-1′), 98.9 (C-2′), 71.9 (C-3′), 70.2 (C-4′), 162.7 (C-5′), 83.9 (C-6′) ppm. HRMS (ESI): calculated for $C_{11}H_{15}N_5O_5$ $[M - H]^-$: 278.0895, found: 278.0900.

Compound **2**: ^{1}H NMR (600 MHz, D_2O) δ 8.35 (s, 1H, H-2), 8.19 (s, 1H, H-8), 4.29 (d, J = 12.7 Hz, 1H, H-1′), 4.13 (d, J = 12.6 Hz, 1H, H-1′), 5.02 (d, J = 4.9 Hz, 1H, H-3′), 4.17 (dd, J = 7.3, 5.1 Hz, 1H, H-4′), 4.26 (m, 1H, H-5′), 3.92 (dd, J = 12.6 Hz, 2.5 Hz, 1H, H-6′), 3.74 (dd, J = 12.8, 5.0 Hz, H-6′) ppm. ^{13}C NMR (150 MHz, D_2O) δ 152.1 (C-2), 147.7 (C-4), 119.6 (C-5), 155.4 (C-6), 140.9 (C-8), 62.1 (C-1′), 97.8 (C-2′), 74.6 (C-3′), 69.6 (C-4′), 83.8 (C-5′), 60.8 (C-6′) ppm. HRMS (ESI): calculated for $C_{11}H_{15}N_5O_5$ $[M - H]^-$: 296.1000, found: 296.1009.

Crystal data for compound **1**: $C_{11}H_{13}N_5O_4 \bullet H_2O$, M = 297.28, a = 10.6769(2) Å, b = 10.6769(2) Å, c = 9.9744(2) Å, α = 90°, β = 90°, γ = 120°, V = 984.71(4) Å^3, T = 100.(2) K, space group *P*32, Z = 3, μ(Cu Kα) = 1.031 mm^{-1}, 17,257 reflections measured, and 2439 independent reflections (R_{int} = 0.0397). The final R_1 values were 0.0244 ($I > 2\sigma(I)$). The final wR (F^2) values were 0.0604 ($I > 2\sigma(I)$). The final R_1 values were 0.0253 (all data). The final wR (F^2) values were 0.0611 (all data). The goodness of fit on F^2 was 1.060. Flack parameter = 0.01(7).

Chemical Synthesis of PMP. To a stirred solution of compound **2** (23 mg, 77.37 μM) in 1 mL of triethyl phosphate was added pyrophosphoryl chloride (77.9 mg, 309.48 μM, 4.0 eq) at −78 °C under argon. The mixture was stirred for 5 h at −78 °C. After that, the reaction mixture was poured into iced water and stirred for 0.5 h at 0 °C. The mixture was then washed with dichloromethane (5 mL, three times), and the aqueous phase was slowly titrated with 1 M NaOH (aq) to about pH 7.0 and then lyophilized. The residual white solid was dissolved in 0.5 mL of ddH_2O and then isolated by analytical HPLC using a Dionex Carbopac PA10 carbohydrate column with water as solvent A and 1.0 M NH_4OAc (aq) as solvent B. Gradient elution was performed with a flow rate of 1 mL/min and UV detection at 260 nm using the following conditions: 0−5 min, 5% solvent B; 5.1−10 min, 20% solvent B; 10.1−15 min, 40% solvent B; 15.1−18 min, 100% solvent B. The eluate at 12.5 min was collected and lyophilized to afford PMP (2.1 mg, 5.57 μM, 7.2% yield) as a

https://doi.org/10.1021/acschembio.2c00739
ACS Chem. Biol. 2023, 18, 102−111

white solid. ^{1}H NMR (800 MHz, D_2O) δ 8.45 (s, 1H, H-2), 8.22 (s, 1H, H-8), 4.34 (d, J = 12.7 Hz, 1H, H-1′), 4.14 (d, J = 12.7 Hz, 1H, H-1′), 5.02 (d, J = 4.7 Hz, 1H, H-3′), 4.29 (dd, J = 7.7, 4.8 Hz, 1H, H-4′), 4.38 (m, 1H, H-5′), 4.22 (m, 1H, H-6′), 4.03 (m, 1H, H-6′) ppm. ^{13}C NMR (200 MHz, D_2O) δ 151.9 (C-2), 147.6 (C-4), 119.8 (C-5), 155.4 (C-6), 141.4 (C-8), 62.3 (C-1′), 97.8 (C-2′), 74.8 (C-3′), 69.2 (C-4′), 82.3 (d, J = 8.7 Hz, C-5′), 63.3 (d, J = 4.3 Hz, C-6′) ppm. ^{31}P NMR (324 MHz, D_2O), δ 3.84 (s) ppm. HRMS (ESI): calculated for $C_{11}H_{15}N_5O_8P$ $[M - H]^-$: 376.0664, found: 376.0671.

Genome Sequencing and Genomic Library Construction. The genome of *S. caniferus* NEAU6 was sequenced by Pacific Biosciences RS II (PacBio RS II) single-molecule real-time (SMRT) technology. Sequencing was performed at the Beijing Novogene Bioinformatics Technology Co., Ltd. (Beijing, China). The low-quality reads were filtered by SMRT 2.3.0[20,21] and the filtered reads were assembled to generate one contig without gaps. According to standard procedures, the genomic DNA was partially digested with *Mbo*I. Then, the 30−45 kb DNA fragments were isolated and ligated to cosmid SuperCos1 or pJTU2554. MaxPlax Lambda packaging extracts were used for packaging. About 2000 *E. coli* clones were picked and stored in 20 96-well microplates at 80 °C.

Gene Inactivation. Primers designed for inactivation of each gene are listed in Table S5. The positive cosmid SuperCos1-3E3 was transformed into *E. coli* BW25113/pIJ790 for gene inactivation. Gene disruption cassette *aac(3)IV-oriT* was amplified using a fragment from plasmid pIJ773 that was digested with *Eco*RI and *Hind*III. PCR products of *aac(3)IV-oriT* cassette for each disrupted gene were electrotransformed into *E. coli* BW25113/pIJ790 containing cosmid 3E3 for λ-RED-mediated recombination to yield recombinant cosmids pSc1136−pSc1146. These recombinant cosmids were transformed into *E. coli* ET12567/pUZ8002 and suffered from intergeneric conjugation with *S. caniferus* NEAU6 wild strain. *E. coli*−*Streptomyces* conjugation was performed on MS solid medium freshly supplemented with 10 mM $MgCl_2$. Double crossover mutants were first selected on the basis of the Kan^SApr^R phenotype and then further confirmed by PCR using primers listed in Table S6. The mutants were fermented using the same conditions as those of wild-type *S. caniferus* NEAU6. The fermentation broth was centrifuged to remove the precipitate and the supernatant was adsorbed by HP-20 resin, which was washed twice with equal volume of water and then eluted with 100% MeOH. The eluent was evaporated under reduced pressure at a temperature within 40 °C and then analyzed by HPLC with CH_3CN−H_2O (5:95, v/v; wavelength 260 nm).

Heterologous Expression. The positive cosmid pJTU2554-10H5 was transferred into *E. coli* ET12567/pUZ8002 and then introduced into *S. coelicolor* M1154 via intergeneric conjugation to generate the *S. coelicolor* M1154/10H5 strain. The colonies were selected with 50 μg/mL apramycin after 5 days cultivation and subsequently identified through PCR with the corresponding primers. The engineered strain *S. coelicolor* M1154/10H5 was fermented using the same conditions as those of wild-type *S. caniferus* NEAU6. The fermentation broth was treated and analyzed in the same way as the mutant strains.

Protein Expression and Purification. The genes encoding GvmA, GvmB, GvmC, GvmD, and GvmE were amplified by PCR from cosmid SuperCos1-3E3 with primers listed in Table S7. *gvmA* and *gvmC* genes were cloned into the pET26b vector, and *gvmB*, *gvmD*, and *gvmE* genes were cloned into the pET28a vector using the *Nde*I and *Hind*III restriction sites. The resulting plasmids were used to transform *E. coli* BL21 (DE3) cells. Recombinant colonies were selected on LB agar plates supplemented with kanamycin (50 μg/mL). Positive clones were identified by colony PCR and the corresponding plasmids were isolated and confirmed by sequencing. Site-mutated pET28a-*gvmE* were obtained by fusion PCR using wild pET28a-*gvmE* as the template and the primers are listed in Table S8.

The *E. coli* BL21 (DE3) cells containing pET26b-*gvmA*, pET26b-*gvmC*, pET28a-*gvmB*, pET28a-*gvmD*, pET28a-*gvmE*, or site-mutated pET28a-*gvmE* were cultured in LB liquid medium supplemented with kanamycin (50 μg/mL) to an OD_{600} of 0.6 at 37 °C. The cultures were cooled on ice for 10 min and induced with 0.25 mM IPTG for 18 h at 16 °C. The cells were centrifuged for 15 min at 4000 rpm at 4 °C and the pellet resuspended in 50 mL of buffer A (Tris 50 mM, NaCl 300 mM, imidazole 15 mM, glycerol 10%, pH 8.0) and homogenized on ice by sonication. The lysates were centrifugated at 24,000 rpm for 1 h and the supernatant was filtered and purified using the AKTA pure system with a 5 mL Histrap TM FF column (GE Healthcare). The samples were eluted by a linear imidazole gradient of buffer A and buffer B (imidazole 500 mM, Tris 50 mM, NaCl 100 mM, pH 8.0). The target proteins were concentrated by ultrafiltration using Amicon Ultra-4 (10 K, Millipore) and stored at −80 °C in the buffer (NaH_2PO_4 100 mM, glycerol 10%, pH 8.0). Protein concentrations were determined using the Bradford method.

***In Vitro* Biochemical Activity of GvmD.** GvmD enzymatic activity was tested in 50 μL volume containing 1 μM GvmD, 1 mM D-fructose 6-phosphate, and 5 mM $MgCl_2$ in 50 mM Tris·HCl (pH 8.0) at 30 °C for 2 h. The reaction was quenched by adding 50 μL of chloroform. After centrifugation to remove the protein, the supernatant was treated with 1 μL of calf intestinal alkaline phosphatase (30 U/μL, Takara) at 37 °C for 1 h. The reaction was quenched by adding 50 μL of chloroform. The reaction mixture was then centrifuged at 12,000 rpm for 10 min and the supernatant was detected by TLC using a solvent mixture of ethanol, chloroform, *n*-butanol, and 25% ammonia water (5:2:4:8, v/v) and then analyzed by LC-MS eluted with CH_3CN−H_2O (70:30, v/v) at a flow rate of 1 mL min^{-1} on HITACHI LaChrom NH2 column (4.6 mm × 250 mm, i.d., 5 μm).

***In Vitro* Biochemical Activities of GvmC and GvmE.** GvmC enzymatic activity was tested in 50 μL volume containing 1 μM GvmD, 1 μM GvmC, 1 mM D-fructose 6-phosphate, 1 mM ATP, 5 mM $MgCl_2$, and 5 mM KPi (pH 8.0) in 50 mM Tris·HCl (pH 8.0) at 30 °C for 2 h. The reaction was quenched by adding 50 μL of chloroform. After centrifugation to remove the protein, the supernatant was subject to HRMS analysis.

The GvmC/GvmE coupled enzymatic activity was tested in 50 μL volume containing 1 μM GvmD, 1 μM GvmC, 1 μM GvmE, 1 mM ATP, 1 mM adenine, 5 mM $MgCl_2$, and 5 mM KPi (pH 8.0) in 50 mM Tris·HCl (pH 8.0) at 30 °C for 2 h. The reactin was quenched by adding 50 μL of chloroform. After centrifugation to remove the protein, the supernatant was subject to HPLC analysis. The target peak was confirmed by HRMS.

The GvmC enzymatic activity against D-ribose 5-phosphate was tested in 50 μL volume containing 1 μM GvmC, 1 mM D-ribose 5-phosphate, 1 mM ATP, 5 mM $MgCl_2$, and 5 mM KPi (pH 8.0) in 50 mM Tris·HCl (pH 8.0) at 30 °C for 2 h. The GvmE enzymatic activity against PRPP was tested in 50 μL volume containing 1 μM GvmE, 1 mM PRPP, 1 mM adenine, and 5 mM $MgCl_2$ in 50 mM Tris·HCl (pH 8.0) at 30 °C for 2 h. The reaction was quenched by adding 50 μL of chloroform. After centrifugation to remove the protein, the supernatant was subject to HPLC analysis.

***In Vitro* Biochemical Activity of GvmB.** GvmB enzymatic activity was tested in 50 μL volume containing 1 μM AngE, 1 mM AMP or PMP, and 5 mM $MgCl_2$ in 50 mM Tris·HCl (pH 8.0) at 30 °C for 1 h. The reaction was quenched by adding 50 μL of methanol. After centrifugation to remove the protein, the supernatant was subject to HPLC analysis eluted with a flow rate of 1 mL min^{-1} over a gradient with H_2O and CH_3CN (t = 0 min, 5% CH_3CN; t = 4 min, 5% CH_3CN; t = 4.1 min, 9% CH_3CN; t = 10 min, 9% CH_3CN; t = 10.1 min, 100% acetonitrile) on a YMC-Triart C 18 column (250 mm × 4.6 mm i.d., 5 μm).

The time courses of GvmB-catalyzed dephosphorylation of AMP and PMP were carried out in 50 μL of the reaction containing 1 μM GvmB, 1 mM AMP, 1 mM PMP, and 5 mM $MgCl_2$ in 50 mM Tris·HCl (pH 8.0) at 30 °C. The reaction mixture was treated and analyzed following the conditions described above.

***In Vitro* Biochemical Activity of GvmA.** GvmA enzymatic activity was tested in 50 μL volume containing 1 μM GvmA and 1 mM AMP or PMP in 50 mM Tris·HCl (pH 8.0) at 30 °C for 1 h. The reaction was quenched by adding 50 μL of methanol. After centrifugation to remove the protein, the supernatant was subject to HPLC analysis.

https://doi.org/10.1021/acschembio.2c00739
ACS Chem. Biol. 2023, 18, 102−111

Kinetic Analyses of GvmA, GvmB, GvmE, and GvmE^{E160L}. Kinetic analysis of GvmA against AMP was performed in the reaction mixture containing 50 mM Tris·HCl (pH 8.0), 10 nM GvmA, and AMP concentrations ranging between 25 and 1000 μM. The kinetic analysis of GvmB against PMP was performed in the reaction mixture containing 50 mM Tris·HCl (pH 8.0), 5 mM $MgCl_2$, 20 nM GvmB, and PMP concentrations ranging between 100 and 2000 μM. The kinetic analysis of GvmB against AMP was performed in the reaction mixture containing 50 mM Tris·HCl (pH 8.0), 5 mM $MgCl_2$, 2.92 μM GvmB, and AMP concentrations ranging between 250 and 5000 μM. The kinetic analysis of GvmE or GvmE^{E160L} against PRPP was performed in the reaction mixture containing 50 mM Tris·HCl (pH 8.0), 40 nM GvmE or 17 μM GvmE^{E160L}, 0.5 mM adenine, 5 mM $MgCl_2$, and PRPP concentrations ranging between 10 and 400 μM. The kinetics was measured by HPLC analysis. All assays were performed in triplicate, and the K_m and V_{max} values were calculated from curve fitting to the Michaelis–Menten equation $V_0 = (V_{max} \times [S])/(K_m + [S])$. The k_{cat} values were calculated according to the equation $k_{cat} = V_{max}/[E]$.

GvmA-E Activity Assay. GvmA-E enzymatic activity was tested in 100 μL volume containing 1 μM individual proteins (GvmA, GvmB, GvmC, GvmD, and GvmE), 1 mM D-fructose 6-phosphate, 1 mM ATP, 5 mM $MgCl_2$, and 5 mM KPi (pH 8.0) in 50 mM Tris·HCl (pH 8.0) at 30 °C for 2 h. The reaction was quenched by adding 100 μL of methanol. After centrifugation to remove the protein, the supernatant was subject to HPLC analysis.

GvmB-E Activity Assay. GvmB-E enzymatic activity was tested in 100 μL volume containing 1 μM individual proteins (GvmB, GvmC, GvmD, and GvmE), 1 mM D-fructose 6-phosphate, 1 mM ATP, 1 mM adenine (or without adenine), 5 mM $MgCl_2$, and 5 mM KPi (pH 8.0) in 50 mM Tris·HCl (pH 8.0) at 30 °C for 2 h. The reaction was quenched by adding 100 μL of methanol. After centrifugation to remove the protein, the supernatant was subject to HPLC analysis.

Crystallization and Structure Determination of GvmE. Crystals of GvmE were grown by the sitting drop vapor diffusion method at 293 K. The drops contained a 1:1 mixture of 9 mg/mL protein and a crystallization buffer (0.1 M MES [pH 6.5], 19% PEG 3350) each. Diffraction data were collected using X-rays at a wavelength of 0.9795 Å and a temperature of 100 K at beamline 18U of the Shanghai Synchrotron Radiation Facility (SSRF) and then processed using HKL3000 software.[22] The structure was solved by the molecular replacement method with starting model PDB entry 6FSP,[23] which has a 47.4% similarity with the GvmE sequence. An initial model was built using PHENIX.autobuild[24] and subject to manual adjustment using COOT[25] with all models refined using PHENIX. Refinement[24] and Refmac5.[26]

■ ASSOCIATED CONTENT

Supporting Information

The Supporting Information is available free of charge at https://pubs.acs.org/doi/10.1021/acschembio.2c00739.

Experimental materials, supplementary figures, and tables, including details on primer sequences, gene cluster analysis, gene deletion and expression, kinetic analysis, NMR spectra, X-ray crystallographic data for guvermectin, and crystal structure of GvmE (PDF)

■ AUTHOR INFORMATION

Corresponding Authors

Xiangjing Wang − *Key Laboratory of Agricultural Microbiology of Heilongjiang Province, Northeast Agricultural University, Harbin 150030, China*; Email: wangneau2013@163.com

Sheng-Xiong Huang − *State Key Laboratory of Phytochemistry and Plant Resources in West China, Kunming Institute of Botany, Chinese Academy of Sciences, Kunming 650201, China*; orcid.org/0000-0002-3616-8556; Email: sxhuang@mail.kib.ac.cn

Wensheng Xiang − *Key Laboratory of Agricultural Microbiology of Heilongjiang Province, Northeast Agricultural University, Harbin 150030, China; State Key Laboratory for Biology of Plant Diseases and Insect Pests, Institute of Plant Protection, Chinese Academy of Agricultural Sciences, Beijing 100193, China*; orcid.org/0000-0002-1826-5985; Email: xiangwensheng@neau.edu.cn

Authors

Chongxi Liu − *Key Laboratory of Agricultural Microbiology of Heilongjiang Province, Northeast Agricultural University, Harbin 150030, China; State Key Laboratory of Phytochemistry and Plant Resources in West China, Kunming Institute of Botany, Chinese Academy of Sciences, Kunming 650201, China*; orcid.org/0000-0002-6505-7820

Zhiyan Wang − *Key Laboratory of Agricultural Microbiology of Heilongjiang Province, Northeast Agricultural University, Harbin 150030, China; State Key Laboratory of Phytochemistry and Plant Resources in West China, Kunming Institute of Botany, Chinese Academy of Sciences, Kunming 650201, China*

Yin Chen − *State Key Laboratory of Phytochemistry and Plant Resources in West China, Kunming Institute of Botany, Chinese Academy of Sciences, Kunming 650201, China*

Yijun Yan − *State Key Laboratory of Phytochemistry and Plant Resources in West China, Kunming Institute of Botany, Chinese Academy of Sciences, Kunming 650201, China*

Lei Li − *Key Laboratory of Agricultural Microbiology of Heilongjiang Province, Northeast Agricultural University, Harbin 150030, China*

Yong-Jiang Wang − *State Key Laboratory of Phytochemistry and Plant Resources in West China, Kunming Institute of Botany, Chinese Academy of Sciences, Kunming 650201, China*

Lu Bai − *Key Laboratory of Agricultural Microbiology of Heilongjiang Province, Northeast Agricultural University, Harbin 150030, China; State Key Laboratory for Biology of Plant Diseases and Insect Pests, Institute of Plant Protection, Chinese Academy of Agricultural Sciences, Beijing 100193, China*

Shanshan Li − *State Key Laboratory for Biology of Plant Diseases and Insect Pests, Institute of Plant Protection, Chinese Academy of Agricultural Sciences, Beijing 100193, China*

Yanyan Zhang − *State Key Laboratory for Biology of Plant Diseases and Insect Pests, Institute of Plant Protection, Chinese Academy of Agricultural Sciences, Beijing 100193, China*

Complete contact information is available at: https://pubs.acs.org/10.1021/acschembio.2c00739

Author Contributions

‖C.L., Z.W., and Y.C. contributed equally to this work.

Notes

The authors declare no competing financial interest.

■ ACKNOWLEDGMENTS

This work was supported by grants from the National Natural Science Foundation of China (31772240, 32030090, and U1702285), the Yunnan Provincial Science and Technology

Department (2019FJ007 and 2019FA034), the Biological Resources Program (KFJ-BRP-009), and the Research Program of Frontier Sciences (QYZDB-SSW-SMC051). The authors appreciated W. Wang from the Institute of Microbiology, Chinese Academy of Sciences, for his suggestions on revising this paper.

REFERENCES

(1) Yuntsen, H.; Ohkuma, K.; Ishii, Y.; Yonehara, H. Studies on angustmycin. III. *J. Antibiot.* **1956**, *9*, 195−201.
(2) Vavra, J. J.; Dietz, A.; Churchill, B. W.; Siminoff, P.; Koepsell, H. J. Psicofuranine. III. Production and biological studies. *Antibiot. Chemother.* **1959**, *9*, 427−431.
(3) Lewis, C.; Reames, H. R.; Rhuland, L. E. Psicofuranine. II. Studies in experimental animal infections. *Antibiot. Chemother.* **1959**, *9*, 421−426.
(4) Bianchi-Smiraglia, A.; Wawrzyniak, J. A.; Bagati, A.; Marvin, E. K.; Ackroyd, J.; Moparthy, S.; Bshara, W.; Fink, E. E.; Foley, C. E.; Morozevich, G. E.; et al. Pharmacological targeting of guanosine monophosphate synthase suppresses melanoma cell invasion and tumorigenicity. *Cell. Death. Differ.* **2015**, *22*, 1858−1864.
(5) Shiraishi, T.; Xia, J.; Kato, T.; Kuzuyama, T. Biosynthesis of the nucleoside antibiotic angustmycins: identification and characterization of the biosynthetic gene cluster reveal unprecedented dehydratase required for exo-glycal formation. *J. Antibiot.* **2021**, *74*, 830−833.
(6) Yu, L.; Zhou, W.; She, Y.; Ma, H.; Cai, Y-S.; Jiang, M.; Deng, Z.; Price, N. P. J.; Chen, W. Efficient biosynthesis of nucleoside cytokinin angustmycin A containing an unusual sugar system. *Nat. Commun.* **2021**, *12*, No. 6633.
(7) Xu, G.; Kong, L.; Gong, R.; Xu, L.; Gao, Y.; Jiang, M.; Cai, Y-S.; Hong, K.; Hu, Y.; Liu, P.; et al. Coordinated biosynthesis of the purine nucleoside antibiotics aristeromycin and coformycin in actinomycetes. *Appl. Environ. Microbiol.* **2018**, *84*, No. e01860-18.
(8) Silva, M.; Silva, C. H. T. P.; Iulek, J.; Oliva, G.; Thiemann, O. H. Crystal structure of adenine phosphoribosyltransferase from *Leishmania tarentolae*: potential implications for APRT catalytic mechanism. *Biochim. Biophys. Acta, Proteins Proteomics* **2004**, *1696*, 31−39.
(9) Gust, B.; Challis, G. L.; Fowler, K.; Kieser, T.; Chater, K. F. PCR-targeted *Streptomyces* gene replacement identifies a protein domain needed for biosynthesis of the sesquiterpene soil odor geosmin. *Proc. Natl. Acad. Sci. U.S.A.* **2003**, *100*, 1541−1546.
(10) Chan, K. K.; Fedorov, A. A.; Fedorov, E. V.; Almo, S. C.; Gerltet, J. A. Structural basis for substrate specificity in phosphate binding (β/α) 8-barrels: D-allulose 6-phosphate 3-epimerase from *Escherichia coli* K-12. *Biochemistry* **2008**, *47*, 9608−9617.
(11) Hove-Jensen, B.; Andersen, K. R.; Kilstrup, M.; Martinussen, J.; Switzer, R. L.; Willemoës, M. Phosphoribosyl diphosphate (PRPP): biosynthesis, enzymology, utilization, and metabolic significance. *Microbiol. Mol. Biol. Rev.* **2016**, *81*, No. e00040-16.
(12) Burroughs, A. M.; Allen, K. N.; Dunaway-Mariano, D.; Aravind, L. Evolutionary genomics of the HAD superfamily: understanding the structural adaptations and catalytic diversity in a superfamily of phosphoesterases and allied enzymes. *J. Mol. Biol.* **2006**, *361*, 1003−1034.
(13) Seo, H.; Kim, K. J. Structural insight into molecular mechanism of cytokinin activating protein from *Pseudomonas aeruginosa* PAO1. *Environ. Microbiol.* **2018**, *20*, 3214−3223.
(14) Huyet, J.; Ozeir, M.; Burgevin, M-C.; Pinson, B.; Chesney, F.; Remy, J-M.; Siddiqi, A. R.; Lupoli, R.; Pinon, G.; Saint-Marc, C.; et al. Structural insights into the forward and reverse enzymatic reactions in human adenine phosphoribosyltransferase. *Cell. Chem. Biol.* **2018**, *25*, 666−676.
(15) Phillips, C. L.; Ullman, B.; Brennan, R. G.; Hill, C. P. Crystal structures of adenine phosphoribosyltransferase from *Leishmania donovani*. *EMBO J.* **1999**, *18*, 3533−3545.
(16) Shi, W.; Tanaka, K. S.; Crother, T. R.; Taylor, M. W.; Almo, S. C.; Schramm, V. L. Structural analysis of adenine phosphoribosyltransferase from *Saccharomyces cerevisiae*. *Biochemistry* **2001**, *40*, 10800−10809.
(17) Shi, W.; Sarver, A. E.; Wang, C. C.; Tanaka, K. S.; Almo, S. C.; Schramm, V. L. Closed site complexes of adenine phosphoribosyltransferase from *Giardia lamblia* reveal a mechanism of ribosyl migration. *J. Biol. Chem.* **2002**, *277*, 39981−39988.
(18) Pavithra, G. C.; Ramagopal, U. A. Crystal structures of APRT from *Francisella tularensis* - an N-H···N hydrogen bond imparts adenine specificity in adenine phosporibosyltransferases. *FEBS J.* **2018**, *285*, 2306−2318.
(19) Jensen, K. F.; Hansen, M. R.; Jensen, K. S.; Christoffersen, S.; Poulsen, J-C. N.; Mølgaard, A.; Kadziola, A. Adenine phosphoribosyltransferase from *Sulfolobus solfataricus* is an enzyme with unusual kinetic properties and a crystal structure that suggests it evolved from a 6-oxopurine phosphoribosyltransferase. *Biochemistry* **2015**, *54*, 2323−2334.
(20) Berlin, K.; Koren, S.; Chin, C. S.; Drake, J. P.; Landolin, J. M.; Phillippy, A. M. Assembling large genomes with single-molecule sequencing and locality-sensitive hashing. *Nat. Biotechnol.* **2015**, *33*, 623−630.
(21) Koren, S.; Phillippy, A. M. One chromosome, one contig: complete microbial genomes from long-read sequencing and assembly. *Curr. Opin. Microbiol.* **2015**, *23*, 110−120.
(22) Minor, W.; Cymborowski, M.; Otwinowski, Z.; Chruszcz, M. HKL−3000: the integration of data reduction and structure solution − from diffraction images to an initial model in minutes. *Acta Crystallogr., Sect. D: Biol. Crystallogr.* **2006**, *62*, 859−866.
(23) Liou, G.; Chiang, Y. C.; Wang, Y.; Weng, J-K. Mechanistic basis for the evolution of chalcone synthase catalytic cysteine reactivity in land plants. *J. Biol. Chem.* **2018**, *293*, 18601−18612.
(24) Adams, P. D.; Afonine, P. V.; Bunkóczi, G.; Chen, V. B.; Davis, I. W.; Echols, N.; Headd, J. J.; Hung, L-W.; Kapral, G. J.; Grosse-Kunstleve, R. W.; et al. PHENIX: a comprehensive python-based system for macromolecular structure solution. *Acta Crystallogr., Sect. D: Biol. Crystallogr.* **2010**, *66*, 213−221.
(25) Emsley, P.; Lohkamp, B.; Scott, W. G.; Cowtan, K. Features and Development of Coot. *Acta Crystallogr., Sect. D: Biol. Crystallogr.* **2010**, *66*, 486−501.
(26) Murshudov, G. N.; Skubak, P.; Lebedev, A. A.; Pannu, N. S.; Steiner, R. A.; Nicholls, R. A.; Winn, M. D.; Long, F.; Vagin, A. A. REFMAC 5 for the refinement of macromolecular crystal structures. *Acta Crystallogr., Sect. D: Biol. Crystallogr.* **2011**, *67*, 355−367.

https://doi.org/10.1021/acschembio.2c00739
ACS Chem. Biol. 2023, 18, 102−111